IEEE Access
Multidisciplinary | Rapid Review | Open Access Journal

Received January 5, 2022, accepted January 24, 2022, date of publication January 31, 2022, date of current version February 10, 2022.

Digital Object Identifier 10.1109/ACCESS.2022.3147382

Robustness Analysis and Controller Design Based on a Generalized Model of Nonisolated Multiphase DC–DC Converter

WEN YAN, LI WEI, (Member, IEEE), DIFU ZHAN, DAN SU, AND MINGRUI ZHANG
Department of Electrical Engineering, Tongji University, Shanghai 200070, China

Corresponding author: Li Wei (weili@tongji.edu.cn)

This work was supported by the National Natural Science Foundation of China under Grant 51777141.

ABSTRACT The nonisolated multiphase dc–dc converter (NMDC) has important research value and broad application prospect in fields such as smart grid and new energy vehicles because of its high power density and low output ripple. However, with the increase of the phase number, the parameter inconsistency among each phase will make the NMDC model quite complex. Moreover, parameter uncertainty and quadratic nonlinearity in the small-signal model can degrade control system performance, leading to a big challenge in controller design. In this paper, the generalized robust control model and the method of robust controller designing of NMDC concerning parameter uncertainty and quadratic nonlinearity is developed. Firstly, parameter uncertainty is described by convex polyhedra model. Secondly, the Lyapunov theorem is applied to solve the linear and quadratic nonlinearity of the control model. Finally, with the method of Linear Matrix Inequality (LMI) region pole configuration, the analytical solution of the control model is achieved. Based on the proposed model, the independent control of NMDC with reduced sensors, including current sharing, flexible power distribution and robust control of the NMDC are realized. Both simulation and experimental results verify the effectiveness of the controller. Compared with traditional controller, the controller proposed in this paper can be stable in more complicated working conditions, and has a faster adjustment time, suitable for multiple topologies as well.

INDEX TERMS Nonisolated multiphase dc–dc converter (NMDC), parameter uncertainty, quadratic nonlinearity, convex polyhedron, robust control.

I. INTRODUCTION

With the rapid development of smart grid and new energy vehicles, high-power density DC-DC converter has become a research hotspot in the field of power electronics. The nonisolated multiphase dc–dc converter(NMDC) not only breaks the power limit of a single device, but also effectively reduces the demand for capacitance and inductance, thus increasing the power density. In addition, lower output ripple, more controllable components and design margin improve the control flexibility and reliability of the DC-DC converter. Therefore, NMDC has important research significance and application value [1]–[6].

However, there are some challenges in the development of NMDC. First of all, the NMDC has a complex structure and many components, which make it difficult to derive the generalized model by the traditional segmentation method, especially when the number of phases exceeds 3 and if non-ideal factors are taken into account. In [1], a three-phase DC-DC converter is analyzed, but the model is only limited to a specific topology and cannot be used for other DC-DC converters with different phase number. The method proposed in [7]–[9] overcomes the topology limitation, but only if the phases are ideally symmetric. In [10] and [11], stray parameters and asymmetry of NMDC are considered, but only steady-state analysis is performed. The main challenge of NMDC modeling is that it is difficult to derive the generalized model by the traditional segmentation method, especially when the number of phases exceeds 3 and if non-ideal factors are taken into account.

The associate editor coordinating the review of this manuscript and approving it for publication was Yonghao Gui.

Secondly, the parameter uncertainty and quadratic nonlinearity of the NMDC affect the stability and reliability of the control. In the design of single-phase DC-DC converters, when the controller based on the linear model changes at the operating point, the deviation of the model parameters and the quadratic nonlinearity will result in reduced system stability and reliability. This problem also exists in NMDC and is more complicated. In [12], [13], the robust control problem of single-phase boost converter is described in detail, and a set of complete solutions is given under the parameter uncertainty and the quadratic nonlinearity. In [14]–[16], the H_∞ method is used to strengthen the anti-interference ability of DC-DC converter. In [17], [18], by establishing a convex polyhedron model with uncertain parameters, the redundant elements of the system are eliminated and the complexity of modeling is reduced. However, the above methods have only considered single-phase or two-phase circuit topologies, which lack applicability analysis for more phases or a general topology.

In [19], a novel switching period averaging method proposed by our research team proposed a NMDC model. This method makes full use of the linear characteristics of the circuit differential function. Without sacrificing accuracy, the modeling process is greatly simplified, and steady-state solution and dynamic small-signal model are derived. Based on result of [19] and robust control theory, the NMDC generalized robust control model and the method of robust controller designing are proposed in this paper. On the basis of general small signal model of NMDC, parameter uncertainty is described by convex polyhedra model, then the Lyapunov theorem is applied to solve the linear and quadratic nonlinearity of the control model. With the method of Linear Matrix Inequality (LMI) region pole configuration, the analytical solution of the control model is achieved.

The novelty of this paper is summarized as follows:

1) A generalized robust control model of NMDC and the method of robust controller design that comprehensively considers parameter uncertainty, disturbance input, and quadratic nonlinearity are proposed.

2) The designed controller has a greater range of stability than other controllers and can cope with more complex working conditions, since the parameter uncertainties are covered in the model, such as duty cycle, output load, input voltage.

3) The designed controller can achieve both current sharing control and flexible power distribution with reduced sensors.

4) The controller model is a generalized model, the designed controller is suitable for single-phase boost, multi-phase boost, multi-phase inductively coupled, multi-phase magnetically integrated and other topologies.

The structure of this paper is as follows: The general model of the NMDC is introduced in Section II. The robust control of the system is analyzed in Section III. The robust controller design method of the NMDC is given in Section IV. Section V verifies that the method has good robust stability and robust performance through simulation and experiments. Finally, Section VI is the conclusion of this paper.

TABLE 1. Topologies with different M, N and L_{mi}.

TOPOLOPY	M	N	L_{mi}
Single-phase Converter	1	1	0
Typical Multiphase Converter	1	>1	0
Coupled Inductor Converter	1	>1	$\neq 0$
Paralleled Coupled Inductor Converter	>1	>1	$\neq 0$

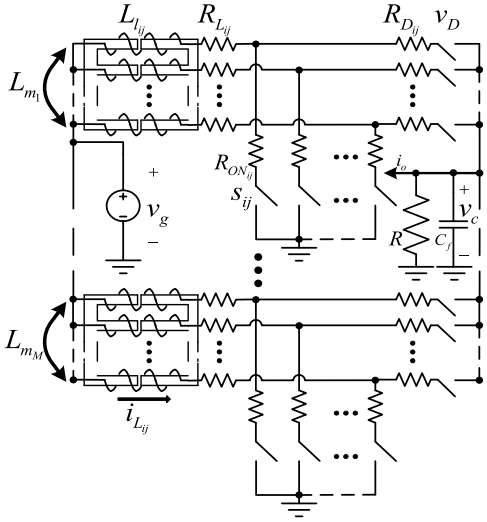

FIGURE 1. Generalized topology of NMBC. The NMDC contains M groups of N-phase coupled inductors connected in parallel.

II. GENERALIZED MODEL OF NMDC

According to [19], the structure of the multi-coupling inductor NMDC shown in Fig. 1 is a general structure, M is the number of coupled inductor groups, N is the number of phases of each group, $L_{mi}(i = 1, 2, \ldots, M)$ is the mutual inductance of group i. When M, N, L_{mi} change, it can transform into a variety of DC-DC converter structures as shown in Table 1.

For the boost converter with the above topologies, according to kirchhoff's law, the circuit differential equation is as follows:

$$\begin{cases} \left(L_{lij} + L_{mi}\right)\dfrac{di_{L_{ij}}(t)}{dt} - L_{mi}\displaystyle\sum_{k=1,k\neq j}^{N}\frac{di_{L_{ik}}(t)}{dt} \\ = v_g(t) - \left[1 - s_{ij}(t)\right]\left[v_c(t) + v_D\right] \\ \quad - \left\{R_{L_{ij}} + s_{ij}(t)R_{ON_{ij}} + \left[1 - s_{ij}(t)\right]R_{D_{ij}}\right\} i_{L_{ij}}(t) \\ C_f\dfrac{dv_c(t)}{dt} = \displaystyle\sum_{i=1}^{M}\sum_{j=1}^{N}\left\{i_{L_{ij}}(t)\left[1 - s_{ij}(t)\right]\right\} - \dfrac{v_c(t)}{R} - i_o(t) \end{cases} \tag{1}$$

where i, j are integers, $i \in [1, M]$, $j \in [1, N]$, and the parameters are defined as shown in Table 2.

TABLE 2. Parameter definition.

parameter	definition
$L_{l_{ij}}$	leakage inductance of phase j, group i
L_{m_i}	mutual inductance of group i
$i_{L_{ij}}(t)$	inductor current of phase j, group i
$v_g(t)$	power source voltage
v_D	diode forward voltage drop
$v_c(t)$	voltage of output capacitor
$R_{D_{ij}}$	diode resistance of phase j, group i
$R_{ON_{ij}}$	switch conduct resistance of phase j, group i
$R_{L_{ij}}$	inductor ESR of phase j, group i
R	load resistance
C_f	output capacitance
i_o	output current
$s_{ij}(t)$	switching state of phase j, group i(0 for ON, 1 for OFF)

Choose all inductor currents and capacitor voltages as state vector:

$$x = \left[i_{L_{11}}(t), \ldots, i_{L_{1N}}(t), i_{L_{21}}(t), \ldots, i_{L_{NM}}(t), v_c(t)\right]^T \quad (2)$$

take input voltage, output current and diode forward voltage drop as interference input vector, whose definition is shown in (3):

$$w = [v_g(t), i_o(t), v_D]^T \quad (3)$$

and combine on-off resistance of MOSFET, on-off resistance of diode and equivalent series resistance into resistive parameter:

$$R_{ij}(d_{ij}) = R_{L_{ij}} + R_{ON_{ij}}d_{ij} + (1 - d_{ij})R_{D_{ij}} \quad (4)$$

With the conclusion of [19], the general small signal model of the NMDC can be obtained:

$$K\frac{d\tilde{x}(t)}{dt} = \bar{A}\tilde{x}(t) + \bar{H}\tilde{D}(t) + \bar{B}\tilde{w}(t) \quad (5)$$

where $D(t)$ is defined as (6), and the definition of matrix A, B, H is in Appendix A. Note that $\bar{A}$ is the steady-state value of A, and $\tilde{A}$ is the ac small signal of A, other variables are all the same.

$$D(t) = [d_{11}(t), \ldots, d_{1N}(t), d_{21}(t), \ldots, d_{MN}(t)]^T \quad (6)$$

III. ROBUST CONTROL ANALYSIS OF NMDC

In practical application, quadratic nonlinearity exists objectively and affects the control performance of the system. Therefore, based on the independent control mode of each group, this section deduces the NMDC control model with quadratic nonlinearity, and analyzes the robust control of the control model.

We modify the dynamic part of the model and retain the second-order nonlinear components:

$$K\dot{\tilde{x}} = \bar{A}\tilde{x} + \bar{B}\tilde{w} + \bar{H}\tilde{D} + \tilde{H}\tilde{D} \quad (7)$$

As the asymmetry between phases of each coupled inductor group is usually not big, here we take the way of independent control of each group, as shown in Fig. 2, where CompM is the outer loop compensator, CompS1 to CompSn

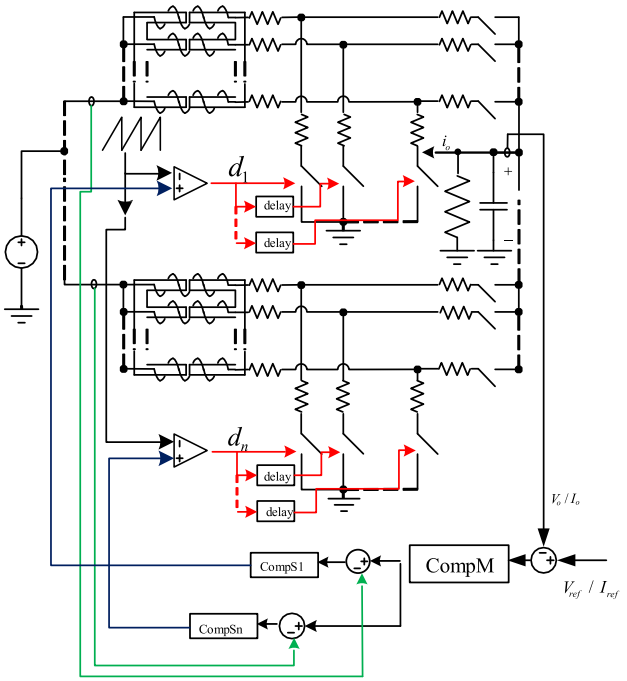

FIGURE 2. Controller structure of each group independently controlled. Each group of coupled inductors share a current sensor and an inner loop compensator.

are inner loop compensators. The frequency response of the inner loop compensator is generated by the outer loop compensator, and duty cycle of each phase in a group is the same. In this way, it can not only achieve current sharing or current prorate control, but also reduce the use of the current sensor.

Based on the above structure, using the method of traditional PID controller design, and increasing M+1 system variables, ξ_i (i = 1,…,M) is the input of inner loop compensator, ξ_{M+1} is the input of outer loop compensator:

$$\begin{cases} \dot{\xi}_1 = \xi_{M+1} - \tilde{i}_{L_1} \\ \vdots \\ \dot{\xi}_M = \xi_{M+1} - \tilde{i}_{L_M} \\ \dot{\xi}_{M+1} = \tilde{v}_{ref} - \tilde{v}_c \end{cases} \quad (8)$$

turn (8) into vector form:

$$\dot{\xi} = k_1\tilde{x} + k_2\xi + k_3\tilde{v}_{ref} \quad (9)$$

then the NMDC with added control variables can be described by the state space form in (10):

$$\dot{\tilde{x}}' = A\tilde{x}' + B_1\tilde{u} + B_r\tilde{r} + B_2\tilde{w} + \tilde{B}_d\tilde{u} \quad (10)$$

where the definition of each matrix and vector is shown in (11), as shown at the bottom of the next page.

It can be seen from (10) that the control model of the NMDC includes an ideal linear model $A\tilde{x} + B_1\tilde{u} + B_r\tilde{r}$, an interference input $B_2\tilde{w}$, and a second-order nonlinear component $\tilde{B}_d\tilde{u}$. Therefore, the following issues need to be considered when designing a NMDC controller.

- Although $A\tilde{x} + B_1\tilde{u} + B_r\tilde{r}$ is an ideal linear model of the system, the relevant parameters in each coefficient matrix are related to the static operating point and device parameters of the converter. The theoretical values are often different from the actual values, therefore, the parameter uncertainty should be considered in closed-loop control system;
- $B_2\tilde{w}$ is the interference input of the system, including the changes of input voltage and load current of NMDC;
- $\tilde{B}_d\tilde{u}$ is a second-order nonlinear component, which is usually ignored in traditional linearization modeling. However, the second-order nonlinear component often leads to deterioration of control performance.

For feedback controller, the following feedback control model is generally used:

$$\tilde{u} = K'\tilde{x}' \tag{12}$$

The key to the robust control of the NMDC is to ensure the stability of the control system and certain control performance in the presence of interference input, nonlinear components, and parameter uncertainty by properly selecting the controller parameters.

IV. ROBUST CONTROLLER DESIGN OF NMDC

Compared with pole configuration [20], PID control, sliding mode control, optimal control, robust control is more adaptable and practical when the system has parameter uncertainty, robust control has therefore attracted widespread attention in the design of power electronic device controllers [17], [21], [22]. PID control is simple and effective, but it is very difficult to find the appropriate control coefficient value for a complex topology like NMDC [23]. Sliding mode control is highly robust, however, the chattering problem in sliding mode control is difficult to eliminate [24]. Optimal control has good output performance, but it is easy to fall into a local optimal solution, and it is less applied to engineering fields that consider stability and reliability [25], [26].

In this section, the robust controller design of NMDC is discussed. Firstly, the convex polyhedron model is used to describe the parameter uncertainty, and then the control method of NMDC is introduced from three aspects: the linear part of the system, the interference input, and the quadratic nonlinearity. Finally, under a certain LMI region of control performance, the algorithm derivation of feedback control parameters is given(Fig. 3).

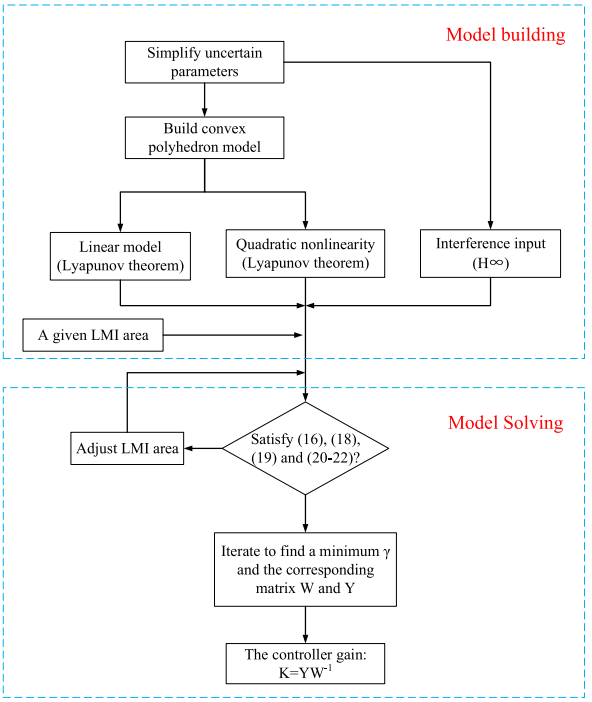

FIGURE 3. Control algorithm flow. The algorithm flow consists of two parts, model building and model solving. Firstly, derive the conditions that need to be met for NMDC robust control from three aspects, and then solve these inequalities.

A. UNCERTAIN PARAMETERS AND CONVEX POLYHEDRON MODEL

In robust control theory, convex polyhedron model is mainly used to describe the parameter uncertainty. Convex polyhedron model means that all possible models are included in a convex polyhedron. Any real system model can be represented by the linear combination of each vertex of the convex polyhedron [27].

It can be seen from (11) that there is no uncertain parameter in Br, because k_3 is a constant or constant matrix in general control system, and the parameter uncertainty of A and B_1 mainly comes from $K^{-1}\bar{A}$ and $K^{-1}\bar{H}$.

The maximum parameter uncertainty in the matrix $K^{-1}\bar{A}$ comes from $\bar{d}_i' = \bar{d}_i - 1$(the duty of each group of coupled inductors is the same, $\bar{d}_{ij}' = \bar{d}_i'$ when $j = 1, \ldots N$), the value of which varies greatly, and the load $\frac{1}{R}$ also changes in a large range between light and heavy loads. In addition, $\bar{R}_{ij}$,

$$\begin{cases} k_1 = \begin{bmatrix} -1 & & \\ & \ddots & \\ & & -1 \end{bmatrix}, k_2 = \begin{bmatrix} 0 & & 0 & 1 \\ & \ddots & & \vdots \\ 0 & & 0 & 1 \\ 0 & \cdots & 0 & 0 \end{bmatrix}, k_3 = \begin{bmatrix} 0 \\ \vdots \\ 0 \\ 1 \end{bmatrix} \\ A = \begin{bmatrix} K^{-1}\bar{A} & 0 \\ k_1 & k_2 \end{bmatrix}, B_1 = \begin{bmatrix} K^{-1}\bar{H} \\ 0 \end{bmatrix}, B_r = \begin{bmatrix} 0 \\ k_3 \end{bmatrix}, B_2 = \begin{bmatrix} K^{-1}\bar{B} \\ 0 \end{bmatrix}, \tilde{B}_d = \begin{bmatrix} K^{-1}\tilde{H} \\ 0 \end{bmatrix}, \tilde{x}' = \begin{bmatrix} \tilde{x} \\ \xi \end{bmatrix}, \tilde{r} = \tilde{v}_{ref} \end{cases} \tag{11}$$

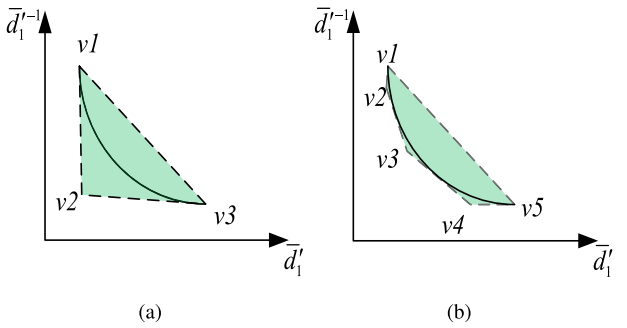

FIGURE 4. Reduce the conservatism of dependent variable groups. (a) is the original triangle region, and (b) is the optimized region.

$\frac{1}{L_{ij}+L_{m_i}}$ as well as $\frac{1}{C_f}$ can be changed with the heat, operating conditions of the NMDC. Actually, the value of capacitance and inductance generally do not change more than 5% during the operation of the converter, which is obviously not as drastic as duty cycle and load resistance. Therefore, they are often ignored.

The range of matrix $K^{-1}\bar{H}$ elements is difficult to determine directly, but it can be estimated. As both $R_{L_{ij}}$ and $R_{ON_{ij}}$ are stray parameters, the value of $\left(R_{L_{ij}} + R_{ON_{ij}}\right) I_{L_{ij}}$ is much smaller than V_g, they can be incorporated into the range of V_g. As for $I_{L_{ij}}$, it can approximated by the conservation of energy shown in (14).

$$\begin{aligned}(V_c + v_D) - \left(R_{ON_{ij}} - R_{D_{ij}}\right) I_{L_{ij}} &= \frac{V_g - \left(R_{L_{ij}} + R_{ON_{ij}}\right) I_{L_{ij}}}{1 - \bar{d}_i} \\ &\approx \frac{V_g}{\bar{d}_i'} \end{aligned} \tag{13}$$

$$I_{L_{ij}} = MN\frac{{V_c}^2}{RV_g} = MN\frac{V_g}{Rd'^2} \tag{14}$$

In summary, the vector of uncertain parameters can be symplified as:

$$\theta = [\bar{d}_1' \cdots \bar{d}_M', \bar{d}_1'^{-1} \cdots \bar{d}_M'^{-1}, \bar{d}_1'^{-2} \cdots \bar{d}_M'^{-2}, \frac{1}{R}, V_g] \tag{15}$$

Since $\bar{d}_i'$, $\bar{d}_i'^{-1}$ and $\bar{d}_i'^{-2}$ are not independent from each other, the convex model has a certain degree of conservativeness. In order to reduce the conservativeness, the method proposed by Olalla C *et al.* and Maccari L *et al.* in [13] and [28] is used in this paper. Find several points on the curve and increase the number of tangents, so that the enclosed area is obviously smaller than the original one, as shown in Fig. 4.

B. ROBUST CONTROL ALGORITHM FOR NMDC

For the robust control of NMDC proposed in section 3, we analyze from linear model, interference input and quadratic nonlinearity respectively, and then, with a given LMI area, how to ensure robust performance is described.

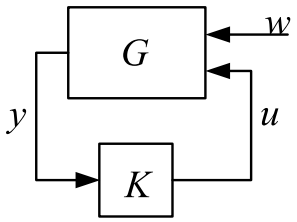

FIGURE 5. Generalized control system.

1) ROBUST STABILITY OF LINEAR MODEL

Considering the linear part, according to lyapunov theory, the system should satisfy the quadratic stability of convex polyhedron model. Based on the feedback control of (12), the robust stable inequality (16) of linear model can be obtained, the derivation process is shown in Appendix B.

$$WA_i^T + A_iW + Y^T{B_i}^T + B_iY < 0, \forall i \tag{16}$$

After solving linear matrix inequality (16), the controller gain can be obtained by $K = YW^{-1}$.

2) ROBUST STABILITY OF INTERFERENCE INPUT

Under the feedback control shown in (12), the influence of the norm-bounded external interference input w on the system output must be minimized(Fig. 5), that is to make the H_∞ norm of the closed-loop transfer function of the interference input to the system output smaller than the given positive number γ [29].

$$\|G\|_\infty = \sup_{\|u\|_2 \neq 0} \frac{\|y\|_2}{\|u\|_2} \tag{17}$$

According to the real bounded lemma, assuming that the change of the reference input $\tilde{r} = 0$ and the quadratic nonlinearity is ignored, when the system output is $y = C\bar{x}$, if positive definite symmetric matrices W and Y can satisfy inequality (18) at all vertices of the convex polyhedron, $\|G\|_\infty < \gamma$ can be achieved, and controller gain can be calculated by $K = YW^{-1}$ [13], [28].

$$\begin{bmatrix} A_iW + WA_i^T + B_iY + Y^TB_i^T & B_2 & WC^T \\ B_2^T & -\gamma I & 0 \\ CW & 0 & -\gamma I \end{bmatrix} < 0 \tag{18}$$

In actual design, the parameter γ needs to be iteratively optimized because a larger γ value often results in no solution of (18), in this case, it is necessary to gradually reduce the value of γ until a numerical solution exists in (18).

3) ROBUST STABILITY OF QUADRATIC NONLINEARITY

Tarbouriech S *et al.* in [30] proposed a control method to stabilize the quadratic nonlinearity, which has the characteristics of small conservatism and large-scale stability. Based on this method, robust control inequality (19) with quadratic nonlinearity is derived, the derivation process is shown in Appendix C.

$$\begin{aligned}(AW + WA^T + \left(B_1 + \left[N_1v_j, \ldots, N_Mv_j\right]\right) Y \\ + Y^T\left(B_1 + \left[N_1v_j, \ldots, N_Mv_j\right]\right)^T) < 0\end{aligned} \tag{19}$$

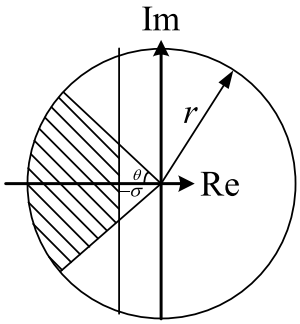

FIGURE 6. Complex LMI area of $S(\sigma, \theta, r)$.

4) ROBOST PERFORMANCE OF LMI AREA

A good control system requires not only good robust stability, but also good robust performance, that is, the pole of the system needs to be located in the designated area. In the problem of pole area allocation, linear matrix inequality can also be useful.

The area that can be expressed by a linear matrix inequality on the complex plane is called the Linear Matrix Inequality (LMI) area. The LMI area $S(\sigma, \theta, r)$ used in this paper is shown in Fig. 6.

Assuming that the system output is $y = C\bar{x}$, when the change of the reference input $\tilde{r} = 0$ and the quadratic nonlinearity is ignored, if positively definite symmetric matrices W and Y can satisfy linear matrix inequality (20-22) at all vertices of the convex polyhedron, all poles of the convex polyhedron system are located in the LMI region $S(\sigma, \theta, r)$, the controller gain can be calculated by $K = YW^{-1}$.

$$A_i W + WA_i^T + B_i Y + Y^T B_i^T + 2\sigma W < 0 \tag{20}$$

$$\begin{bmatrix} -rW & A_i W + B_i Y \\ WA_i^T + Y^T B_i^T & -rW \end{bmatrix} < 0 \tag{21}$$

Above all, in a given LMI area of control performance, if there are a minimum γ and the corresponding symmetric positive definite symmetric matrix W and matrix Y that satisfy the linear matrix inequality (16), (18), (19) and (20-22), then the NMDC control system using the feedback control law of (12) is progressively stable, and feedback control coefficient can be obtained by solving $K = YW^{-1}$.

V. VERIFICATION

Aiming to verificate the design method of the robust controller of the NMDC proposed in the fourth part, simulation and experiment are carried out in this part. The parameters of the converter are shown in Table 3 and 4.

TABLE 3. Range of uncertainty parameters.

parameter	maximum	minimum
d_1'	0.8	0.5
R^{-1}	1/12	1/20
V_g	80	60
V_c	120	100

TABLE 4. Simulation parameters.

parameter	value	parameter	value	parameter	value
$L_{l_{11}}$	$28\mu H$	$L_{l_{12}}$	$28\mu H$	$L_{l_{21}}$	$28\mu H$
$L_{l_{22}}$	$28\mu H$	L_{m_1}	$7.7\mu H$	L_{m_2}	$7.7\mu H$
$R_{l_{11}}$	$29m\Omega$	$R_{l_{12}}$	$21m\Omega$	$R_{l_{21}}$	$23m\Omega$
$R_{l_{22}}$	$32m\Omega$	v_D	0.937V	$R_{ON_{11}}$	$34.5m\Omega$
$R_{ON_{12}}$	$34.5m\Omega$	$R_{ON_{21}}$	$34.5m\Omega$	$R_{ON_{22}}$	$34.5m\Omega$
$R_{D_{11}}$	$10m\Omega$	$R_{D_{12}}$	$10m\Omega$	$R_{D_{21}}$	$10m\Omega$
$R_{D_{22}}$	$10m\Omega$	C_f	$521\mu F$	R	2.232Ω

TABLE 5. The vertices of the parameter uncertainty model.

	$\bar{d}_1'$	$\bar{d}_1'^{-1}$	$\bar{d}_1'^{-2}$	R^{-1}	V_g
v_1	0.5000	2.0000	4.0000	0.0833	60.0000
v_2	0.5000	2.0000	4.0000	0.0833	80.0000
v_3	0.5000	2.0000	4.0000	0.0500	60.0000
v_4	0.5000	2.0000	4.0000	0.0500	80.0000
v_5	0.6047	1.5814	2.3256	0.0833	60.0000
v_6	0.6047	1.5814	2.3256	0.0833	80.0000
v_7	0.6047	1.5814	2.3256	0.0500	60.0000
v_8	0.6047	1.5814	2.3256	0.0500	80.0000
v_9	0.6047	1.7384	2.3256	0.0833	60.0000
v_{10}	0.6047	1.7384	2.3256	0.0833	80.0000
v_{11}	0.6047	1.7384	2.3256	0.0500	60.0000
v_{12}	0.6047	1.7384	2.3256	0.0500	80.0000
v_{13}	0.8000	1.2500	1.5625	0.0833	60.0000
v_{14}	0.8000	1.2500	1.5625	0.0833	80.0000
v_{15}	0.8000	1.2500	1.5625	0.0500	60.0000
v_{16}	0.8000	1.2500	1.5625	0.0500	80.0000

TABLE 6. Polyhedron vertices with quadratic nonlinearity.

	$\tilde{v}_g$	$\tilde{i}_{L_1}$	$\tilde{i}_{L_2}$
v_1	20	6.875	6.875
v_2	20	6.875	-6.875
v_3	20	-6.875	6.875
v_4	20	-6.875	-6.875
v_5	-20	6.875	6.875
v_6	-20	6.875	-6.875
v_7	-20	-6.875	6.875
v_8	-20	-6.875	-6.875

According to the method of reducing conservativeness of correlation variables introduced in Section IV, if the tangent of the endpoint is taken, the corresponding convex polyhedron has 16 vertices, as shown in Table 5.

Assuming that performance parameter $S(\sigma, \theta, r)$ is (10000, 50°,1 × 105), then we need to find W and Y satisfying linear matrix inequalities (16), (18) and (20-22), as shown at the bottom of the page, at 16 vertices, a total of 16 × 5 = 80 inequalities.

$$\begin{bmatrix} \left(A_i W + WA_i^T + B_i Y + Y^T B_i^T\right)\sin\theta & \left(A_i W - WA_i^T + B_i Y - Y^T B_i^T\right)\cos\theta \\ \left(-A_i W + WA_i^T - B_i Y + Y^T B_i^T\right)\cos\theta & \left(A_i W + WA_i^T + B_i Y + Y^T B_i^T\right)\sin\theta \end{bmatrix} < 0 \tag{22}$$

$$G = \begin{bmatrix} -0.0708 & -0.0215 & -0.0446 & 149.4235 & -116.5710 & 830.7025 \\ -0.0215 & -0.0708 & -0.0446 & -116.5710 & 149.4235 & 830.7025 \end{bmatrix} \tag{23}$$

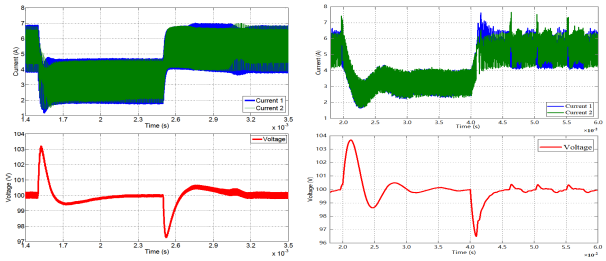

FIGURE 7. Current and voltage waveforms of robust control (a) and PID control (b) with sudden load changes. The input voltage is 80V, the output voltage is 100V. The green and blue waveforms are the currents of the two groups of coupled inductors, the red waveform is the output voltage. The load at the beginning of the simulation is 12Ω, jumps to 20Ω at 1.5ms, and 12Ω at 2.5ms for robust control. As for PID control, the jump time points are 20ms and 40ms.

In addition, the quadratic nonlinearity of the model should be considered. According to the principle of the previous section, we need to find a μ which can contain the maximum quadratic nonlinear range. The minimum input current of the converter is 500w/80v $=$ 6.25A, maximum input current is 1200w/60v $=$ 20A, both of which are divided into two roads, then, the range of current variation in each group is $\pm$6.875 A, the range of output voltage variation is $\pm$20V. So the circuit model of quadratic nonlinearity can be expressed in $\mu = [6.875, 6.875, 20]^T$, and the nonlinear convex polyhedron model corresponding to (19) as shown in Table 6 has 8 vertices.

Based on the 16 vertices of the parameter uncertainty model in Table 5, each quadratic nonlinear vertex needs to satisfy the linear matrix inequality (19), thus a total of 16×8.128 linear matrix inequalitie need to be satisfied to ensure the quadratic stability of the system. Coupled with 80 linear matrix inequalities that satisfy the performance robustness of convex polyhedron, the entire optimization is composed of 208 linear matrix inequalities, that is, the robust control of NMDC is to find the minimum γ and the corresponding matrices W and Y that can satisfy 208 linear matrix inequalities. Calculated by MATLAB LMI toolbox, we get $\gamma = 49.1089$, and the corresponding feedback gain is show in (23), as shown at the bottom of the previous page.

A. SIMULATION

Building the NMDC simulation model with MATLAB/Simulink tool, and in order to verify the effectiveness of the control algorithm proposed in this paper, here we compare it with the conventional PID control, the simulation results are shown in Fig. 7, 8, 9, where (a) is the waveform of robust control proposed in this paper, and (b) is the waveform of PID control.

Under various operating conditions, the output voltage caused by a wide range of load and input voltage changed does not exceed 5%, and the system has a good followability when the given changes widely, in which robust control and PID control are equally good. In addition, the adjustment time of robust control is less than 0.5 ms, the currents of the two groups of coupled inductors are balanced. Conventional PID regulation does not perform very well in this case, as we can see from the waveforms, the regulation time of PID is about 5ms, which is ten times longer than that of robust control. And as shown in 7 (b) and 8 (b), when load changes or output voltage changes, periodic fluctuations in PID control's current occur, which can affect the stability of the system.

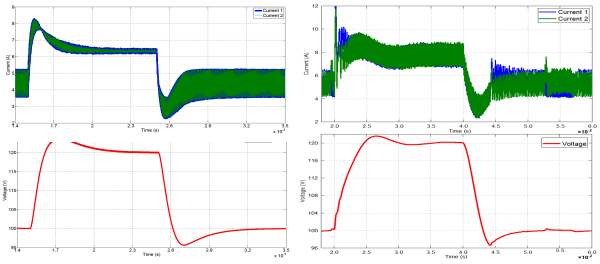

FIGURE 8. Current and voltage waveforms of robust control (a) and PID control (b) with sudden changes of given ouput. The input voltage is 80V, the loads is 12Ω. The green and blue waveforms are the currents of the two groups of coupled inductors, the red waveform is the output voltage. The given output at the beginning of the simulation is 100V, jumps to 120V at 1.5ms, and 100V at 2.5ms for robust control. As for PID control, the jump time points are 20ms and 40ms.

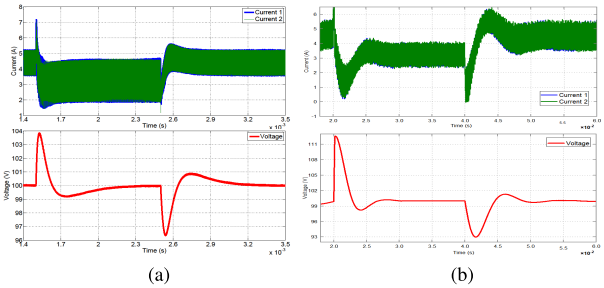

FIGURE 9. Current and voltage waveforms of robust control (a) and PID control (b) with sudden changes of power supply voltage. The output voltage is 100V and, the loads are 20Ω. The green and blue waveforms are the currents of the two groups of coupled inductors, the red waveform is the output voltage. The input voltage at the beginning of the simulation is 60V, jumps to 80V at 1.5ms, and 60V at 2.5ms for robust control. As for PID control, the jump time points are 20ms and 40ms.

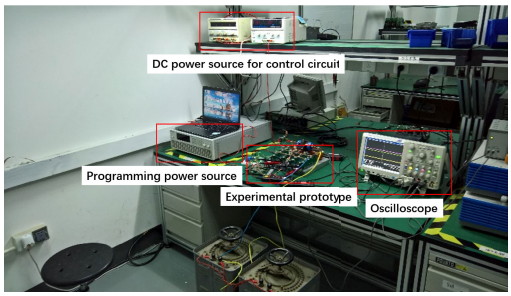

FIGURE 10. Experimental platform.

B. EXPERIMENT

To verify the effectiveness of the proposed control method, we developed a four-phase parallel boost converter (Fig. 11), and two phases making a group share a coupled inductor and a current sensor. The control circuit is based on the structure

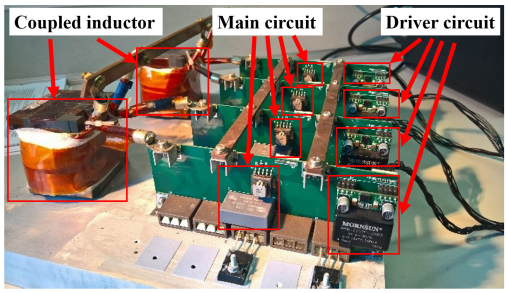

FIGURE 11. The four-phase converter with two coupled inductors.

TABLE 7. Components used in the prototype of this paper.

Component	Model	Manufacturer
Driver power	WRB1215ZP-3WR2	MORNSUN
Driver chip	UCC27201A-Q1	TI
Mosfet	FDBL86366-F085	ONSEMI
DSP	TMS320F28335	TI
FPGA	A3PN125	Micosemi

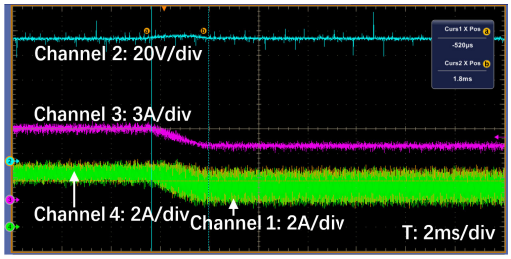

(a)

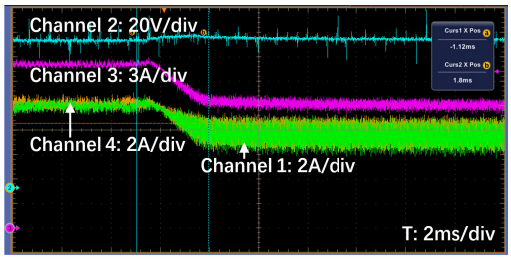

(b)

FIGURE 12. Current and voltage waveforms of input voltage mutation under various operating conditions. The output voltages of (a), (b) are 100V and 120V, the loads are 20Ω and 12Ω respectively. Channel 1 and 4 are the current of the two groups of coupled inductors, channel 2 is the output voltage, channel 3 is the total input current of the converter. The supply voltage changes from 60V to 80V.

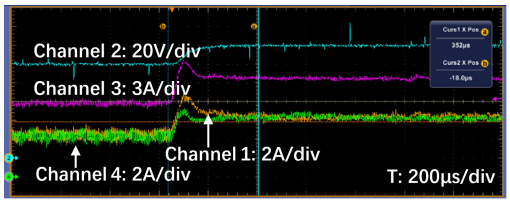

(a)

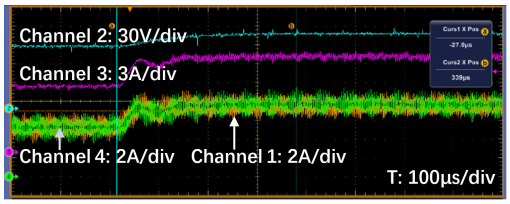

(b)

FIGURE 13. Current and voltage waveforms of output voltage mutation under various operating conditions. The input voltages of (a), (b) are 60V and 80V, the loads are 20Ω and 12Ω respectively. Channel 1 and 4 are the current of the two groups of coupled inductors, channel 2 is the output voltage, channel 3 is the total input current of the converter. The output voltage changes from 100V to 120V.

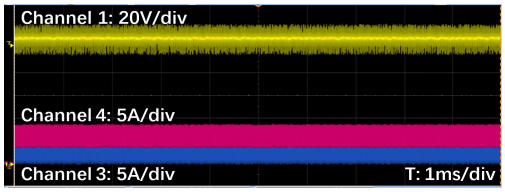

(a)

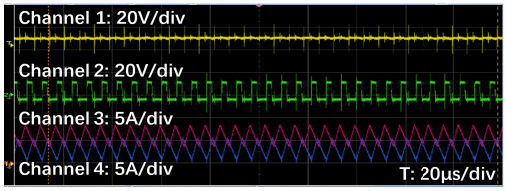

(b)

FIGURE 14. Current and voltage waveforms with two-phase power distribution ratio of 1:2. The input voltage, output voltage and load of (a), (b) are 70V, 110V, 20Ω. Channel 1 is the output voltage, channel 2 and channel 3 are the current of the two phases of coupled inductors, channel 4 is the driving voltage of Mosfet.

of DSP+FPGA. The experimental setup (as shown in Fig. 10) consists of a programmable power supply, an auxiliary dc power supply for the control circuit, and the experimental prototype. The components used in this paper are listed in Table 7.

The experimental results are shown in Fig. 12, 13, 14. Fig. 12 and Fig 13 are experimental waveforms for sudden changes in input voltage and in output voltage respectively. When the input voltage changes abruptly, the output voltage hardly changes. When the given voltage jumps, the output voltage follows quickly, and the adjustment time is around 1ms, the currents of the two groups of coupled inductors are balanced. Fig. 14 is the experimental waveforms with two-phase power distribution ratio of 1:2, from which we can tell the current ratio of two phases with one current sensor is 1:2, and the system can flexibly distribute the power of each phase according to the requirements, and at the same time stays stable.

C. DISCUSSION

With the controller structure and control algorithm proposed in Section IV, the NMDC has good robust stability and performance. Besides, by adopting independent control method, current sharing control and flexible power distribution with reduced sensors are well realized. It can be seen from the simulation and experimental results that the current change of the experiment is slower than that of the simulation, which is the result of slow step response of the power supply

voltage used in experiment and the discretization of control algorithm. However, compared with the adjustment time of tens millisecond of traditional control methods such as PID, the method proposed in this paper has a faster response, moreover, robust control is also more stable against sudden changes.

VI. CONCLUSION

In this paper, based on the generalized DC-DC model proposed in [19], a generalized robust control model of NMDC and the method of robust controller design with parameter uncertainty, system interference input and quadratic nonlinearity are proposed. The designed robust controller not only realize current sharing control with reduced sensors, but also can flexibly distribute power among phases of coupled inductors, and has good stability in the whole operating condition. Compared with traditional control methods, it has a faster dynamic adjustment time, higher stability for large changes in working condition, and moreover, it can be extended to multi-phase converters with multiple structures.

This paper only deduces and designs the robust controller for boost topology. Although the specific formulas are different, the topological modeling process of other NMDC is the same. With the design process and method in this paper, controllers for other topologies can also be implemented.

APPENDIX A
DEFINITION OF MATRICES K, A, B AND $\bar{H}$

$$B = \begin{bmatrix} 1 & 0 & d_{11}-1 \\ \vdots & \vdots & \vdots \\ 1 & 0 & d_{MN}-1 \\ 0 & -1 & 0 \end{bmatrix},$$

and

$$A = \begin{bmatrix} -A_1 & & & -C_1 \\ & \ddots & & \vdots \\ & & -A_M & -C_M \\ C_1^T & \dots & C_M^T & -\frac{1}{R} \end{bmatrix}.$$

Empty elements are zero. The block matrix elements A_i and C_i are defined as

$$A_i = \begin{bmatrix} R_{i1}(d_{i1}) & & \\ & \ddots & \\ & & R_{iN}(d_{iN}) \end{bmatrix},$$
$$C_i = \begin{bmatrix} 1-d_{i1} & \dots & 1-d_{iN} \end{bmatrix}^T.$$

The structure of matrix K is

$$K = \begin{bmatrix} K_1 & & & \\ & \ddots & & \\ & & K_M & \\ & & & C_f \end{bmatrix},$$

Empty block elements are zero. The block element K_i on diagonal is

$$K_i = \begin{bmatrix} L_{l_{i1}} + L_{m_i} & & \\ & \ddots & \\ & & L_{l_{iN}} + L_{m_i} \end{bmatrix}.$$

and empty elements are $-L_{m_i}$.

The derivation of $\bar{H}$ is

$$\begin{aligned} \tilde{A}(t)\bar{x} + \tilde{B}(t)\bar{w} &= \{A[\bar{D} + \tilde{D}(t)] - A(\bar{D})\}\bar{x} \\ &\quad + \{B[\bar{D} + \tilde{D}(t)] - B(\bar{D})\}\bar{w} \\ &= \bar{H}\tilde{D}(t) \end{aligned}$$

and

$$\bar{H} = \begin{bmatrix} V_{11} & & & & & \\ & \ddots & & & & \\ & & V_{1N} & & & \\ & & & V_{21} & & \\ & & & & \ddots & \\ & & & & & V_{MN} \\ -I_{L_{11}} & \dots & -I_{L_{1N}} & -I_{L_{21}} & \dots & -I_{L_{MN}} \end{bmatrix}.$$

where

$$V_{ij} = V_c - (R_{ON_{ij}} - R_{D_{ij}})I_{L_{ij}} + v_D$$

V_c and $I_{L_{ij}}$ are steady-state solutions calculated by (1).

APPENDIX B
DERIVATION OF INEQUALITY (16)

Under the feedback control of (12), the state equation of linear model can witten as

$$\dot{x} = (A + B_1 K)\, x \tag{B.1}$$

Select the quadratic lyapunov function $V = x^T P x$, we can get

$$\begin{aligned} \dot{V} &= \dot{x}^T P x + x^T P \dot{x} \\ &= x^T \left[(A + B_1 K)^T P + P\,(A + B_1 K) \right] x \end{aligned} \tag{B.2}$$

Considering the parameter uncertainty of the system, the sufficient condition for the asymptotic stability of the system is that all vertices of the convex polyhedron satisfy $\dot{V} < 0$, that is, there is a positive definite matrix P that satisfies

$$[A(\theta_i) + B_1(\theta_i)K]^T P + P\,[A(\theta_i) + B_1(\theta_i)K] < 0 \tag{B.3}$$

For convenience, we use A_i instead of $A(\theta_i)$, B_i instead of $B_1(\theta_i)$. Multiplying $W = P^{-1}$ on both sides, we get

$$WA_i^T + A_i W + (KW)^T B_i{}^T + B_i K W < 0, \quad \forall i \tag{B.4}$$

where

$$W = P^{-1}, \quad Y = KW \Leftrightarrow K = YW^{-1} \tag{B.5}$$

APPENDIX C
DERIVATION OF INEQUALITY (19)

The quadratic nonlinear model is shown below

$$\tilde{B}_d\tilde{u} = \begin{bmatrix} \dfrac{N\tilde{v}_c - (R_{ON_1} - R_{D_1})\tilde{i}_{L_1}}{L_{l_1} + (2-N)L_{m_1}}\tilde{d}_1 \\ \vdots \\ \dfrac{N\tilde{v}_c - (R_{ON_M} - R_{D_M})\tilde{i}_{L_M}}{L_{l_M} + (2-N)L_{m_M}}\tilde{d}_M \\ \dfrac{-\sum_{j=1}^{M}\tilde{i}_{L_j}\tilde{d}_j}{C_f} \\ 0 \end{bmatrix} \tag{C.1}$$

for simplification, (C.1) can be written as

$$\tilde{B}_d\tilde{u} = \sum_{j=1}^{M} N_j\tilde{x}\tilde{d}_j \tag{C.2}$$

where N_j is coefficient matrix that can be obtained by (C.2).

Using convex polyhedron to describe the quadratic nonlinear components, the vertices of the convex polyhedron are shown in (C.3):

$$\chi(\tilde{x}) = co\{v_j, j = 1, \ldots, k\} \tag{C.3}$$

All the vertices in the convex polyhedron can be represented by (C.4)

$$\tilde{x} = \sum_{j=1}^{k} \beta_j v_j \tag{C.4}$$

where β is expressed as

$$\sum_{j=1}^{k} \beta_j = 1, \quad \beta_j \geq 0 \tag{C.5}$$

The quadratic nonlinear components usually change near a certain operating point, so $\chi(\tilde{x})$ is a range that's symmetric about the origin as shown in (C.6):

$$\chi(\tilde{x}) = \left\{\tilde{x} \in R^n; -\mu \leq \tilde{x} \leq \mu\right\} \tag{C.6}$$

where $\mu > 0$.

Then the vertices of the convex polyhedron can be represented by the combination of $\tilde{x}$'s upper and lower bounds, such as (C.7):

$$v_j = \Delta_j\mu \tag{C.7}$$

where Δ_j is a diagonal matrix composed of all possible combinations of ± 1.

In summary, the quadratic nonlinear components of the NMDC can be expressed as (C.8):

$$\left[N_1\tilde{x}, \ldots, N_M\tilde{x}\right]\tilde{D} = \left\{\sum_{j=1}^{k} \beta_j \left[N_1 v_j, \ldots, N_M v_j\right]\right\}\tilde{D} \tag{C.8}$$

Next, according to Lyapunov's theorem, building the controller of the NMDC with quadratic nonlinear components.

Selecting $V(\tilde{x}) = \tilde{x}^T P\tilde{x}$ as the quadratic lyapunov function, then its derivative expression under the feedback control law in (12) is as shown in (C.9).

$$\begin{aligned} \dot{V}(\tilde{x}) = \tilde{x}^T\left(PA + A^T P\right)\tilde{x} + \tilde{x}^T\Big[P\left(B_1 + \left[N_1\tilde{x}, \ldots, N_M\tilde{x}\right]\right) \\ \times K + K^T\left(B_1 + \left[N_1\tilde{x}, \ldots, N_M\tilde{x}\right]\right)^T P\Big]\tilde{x} \end{aligned} \tag{C.9}$$

$$\begin{aligned} &(PA + A^T P + P\left(B_1 + \left[N_1 v_j, \ldots, N_M v_j\right]\right)K \\ &+K^T\left(B_1 + \left[N_1 v_j, \ldots, N_M v_j\right]\right)^T P) < 0, \quad j = 1, \ldots, k \end{aligned} \tag{C.10}$$

According to the derivation of quadratic stability of linear part, it is obvious that as long as positive definite symmetric matrix P and control gain K satisfy (C.10), (C.9) can be guaranteed.

Finally, the robust control matrix inequality (19) with quadratic nonlinearity is obtained by transformation like (B.5).

REFERENCES

[1] S. Chandrasekaran and L. U. Gokdere, "Integrated magnetics for interleaved DC–DC boost converter for fuel cell powered vehicles," in *Proc. IEEE 35th Annu. Power Electron. Specialists Conf.*, vol. 1, Jun. 2004, pp. 356–361.

[2] J. Czogalla, J. Li, and C. R. Sullivan, "Automotive application of multi-phase coupled-inductor DC–DC converter," in *Proc. 38th IAS Annu. Meeting Conf. Rec. Ind. Appl. Conf.*, vol. 3, Oct. 2003, pp. 1524–1529.

[3] P.-W. Lee, Y.-S. Lee, D. K. W. Cheng, and X.-C. Liu, "Steady-state analysis of an interleaved boost converter with coupled inductors," *IEEE Trans. Ind. Electron.*, vol. 47, no. 4, pp. 787–795, Aug. 2000.

[4] S. Prabhakaran, C. R. Sullivan, T. O'Donnell, M. Brunet, and S. Roy, "Microfabricated coupled inductors for DC–DC converters for microprocessor power delivery," in *Proc. IEEE 35th Annu. Power Electron. Specialists Conf.*, vol. 6, Jun. 2004, pp. 4467–4472.

[5] W. Wu, N.-C. Lee, and G. Schuellein, "Multi-phase buck converter design with two-phase coupled inductors," in *Proc. 21st Annu. IEEE Appl. Power Electron. Conf. Exposit.*, Mar. 2006, pp. 1–6.

[6] W. Yu, H. Qian, and J. Lai, "Design of high-efficiency bidirectional DC–DC converter and high-precision efficiency measurement," *IEEE Trans. Power Electron.*, vol. 25, no. 3, pp. 650–658, Oct. 2010.

[7] W. Du, H. H. C. Iu, W. Wang, and C. Wang, "Modeling and implementation of a digitally controlled multiphase DC–DC converter," in *Proc. Australas. Universities Power Eng. Conf.*, 2009, pp. 1–6.

[8] O. Hegazy, J. Van Mierlo, and P. Lataire, "Analysis, modeling, and implementation of a multidevice interleaved DC/DC converter for fuel cell hybrid electric vehicles," *IEEE Trans. Power Electron.*, vol. 27, no. 11, pp. 4445–4458, Nov. 2012.

[9] Y.-P. Su, W.-C. Chen, Y.-P. Huang, Y.-H. Lee, K.-H. Chen, and H.-Y. Luo, "Pseudo-ramp current balance (PRCB) technique with offset cancellation control (OCC) in dual-phase DC–DC buck converter," *IEEE Trans. Very Large Scale Integr. (VLSI) Syst.*, vol. 22, no. 10, pp. 2192–2205, Oct. 2014.

[10] S. Zhang and X. Yu, "A unified analytical modeling of the interleaved pulse width modulation (PWM) DC–DC converter and its applications," *IEEE Trans. Power Electron.*, vol. 28, no. 11, pp. 5147–5158, Nov. 2013.

[11] R. L. Andersen and I. Barbi, "A ZVS-PWM three-phase current-fed push–pull DC–DC converter," *IEEE Trans. Ind. Electron.*, vol. 60, no. 3, pp. 838–847, Mar. 2013.

[12] C. Olalla, I. Queinnec, R. Leyva, and A. El Aroudi, "Optimal state-feedback control of bilinear DC–DC converters with guaranteed regions of stability," *IEEE Trans. Ind. Electron.*, vol. 59, no. 10, pp. 3868–3880, Oct. 2012.

[13] C. Olalla, R. Leyva, I. Queinnec, and D. Maksimovic, "Robust gain-scheduled control of switched-mode DC–DC converters," *IEEE Trans. Power Electron.*, vol. 27, no. 6, pp. 3006–3019, Jun. 2012.

[14] A. Qamar, A. U. Awan, K. F. A. Khan, and M. Liaquat, "Scenario based approach for control design for DC–DC buck converter," in *Proc. Int. Conf. Control, Autom. Robot.*, May 2015, pp. 97–102.

[15] G. Rigatos, P. Siano, and C. Cecati, "An H-infinity feedback control approach for three-phase voltage source converters," in *Proc. IECON-40th Annu. Conf. IEEE Ind. Electron. Soc.*, Oct. 2014, pp. 1227–1232.
[16] L. A. Maccari, V. F. Montagner, and A. A. Ferreira, "A linear quadratic control applied to buck converters with H-infinity constraints," in *Proc. Brazilian Power Electron. Conf.*, Oct. 2013, pp. 339–344.
[17] M. A. Bolender, "An overview on dynamics and controls modelling of hypersonic vehicles," in *Proc. Amer. Control Conf.*, 2009, pp. 2507–2512.
[18] H. Sartipizadeh and T. L. Vincent, "A new robust MPC using an approximate convex hull," *Automatica*, vol. 92, pp. 115–122, Jun. 2018.
[19] D. Zhan, L. Wei, Y. Zhang, and Y. Yao, "A generalized model of nonisolated multiphase DC–DC converter based on novel switching period averaging method," *IEEE Trans. Power Electron.*, vol. 30, no. 9, pp. 5181–5191, Sep. 2015.
[20] V. Chapparya, P. Dwivedi, and S. Bose, "Multiphase DC–DC boost converter: Introduction to controller design," in *Transactions on Engineering Technologies*, S.-I. Ao, H. K. Kim, O. Castillo, A. H.-s. Chan, and H. Katagiri, Eds. Singapore: Springer, 2020, pp. 39–53.
[21] H. Sartipizadeh and F. Harirchi, "Robust model predictive control of DC–DC floating interleaved boost converter under uncertainty," in *Proc. 9th Annu. IEEE Green Technol. Conf. (GreenTech)*, Mar. 2017, pp. 320–327.
[22] M. Aguirre, S. Kouro, J. Rodriguez, and H. Abu-Rub, "Model predictive control of interleaved boost converters for synchronous generator wind energy conversion systems," in *Proc. IEEE Int. Conf. Ind. Technol. (ICIT)*, Mar. 2015, pp. 2295–2301.
[23] Y. Adachi, Y. Mochizuki, K. Higuchi, K. Jirasereeamornkul, and K. Chamnongthai, "Design of approximate 2DOF digital controller for interleaved PFC boost converter," in *Proc. Int. Electr. Eng. Congr. (iEECON)*, Mar. 2014, pp. 1–4.
[24] A. Cid-Pastor, R. Giral, J. Calvente, V. I. Utkin, and L. Martinez-Salamero, "Interleaved converters based on sliding-mode control in a ring configuration," *IEEE Trans. Circuits Syst. I, Reg. Papers*, vol. 58, no. 10, pp. 2566–2577, Oct. 2011.
[25] S. Banerjee, A. Ghosh, and N. Rana, "An improved interleaved boost converter with PSO-based optimal type-III controller," *IEEE J. Emerg. Sel. Topics Power Electron.*, vol. 5, no. 1, pp. 323–337, Mar. 2017.
[26] S. Banerjee, A. Ghosh, and N. Rana, "Design and fabrication of closed loop two-phase interleaved boost converter with type-III controller," in *Proc. IECON-42nd Annu. Conf. IEEE Ind. Electron. Soc.*, Oct. 2016, pp. 3331–3336.
[27] C. Olalla, R. Leyva, A. E. Aroudi, P. Garces, and I. Queinnec, "LMI robust control design for boost PWM converters," *IET Power Electron.*, vol. 3, no. 1, pp. 75–85, Jan. 2010.
[28] L. A. Maccari, J. R. Massing, L. Schuch, C. Rech, H. Pinheiro, R. C. L. F. Oliveira, and V. F. Montagner, "LMI-based control for grid-connected converters with LCL filters under uncertain parameters," *IEEE Trans. Power Electron.*, vol. 29, no. 7, pp. 3776–3785, Jul. 2014.
[29] M. Chilali and P. Gahinet, "$H\infty$ design with pole placement constraints: An LMI approach," *IEEE Trans. Autom. Control*, vol. 41, no. 3, pp. 358–367, Mar. 1996.
[30] S. Tarbouriech, I. Queinnec, T. R. Calliero, and P. L. D. Peres, "Control design for bilinear systems with a guaranteed region of stability: An LMI-based approach," in *Proc. 17th Medit. Conf. Control Autom.*, Jun. 2009, pp. 809–814.

WEN YAN received the B.S. degree in ocean resource developing technology from Tongji University, Shanghai, China, in 2019, where he is currently pursuing the M.S. degree in electrical engineering.

His research interests include research and development of high-power density converter for electric vehicle, including modeling and control of converters, and multiphase parallel technique.

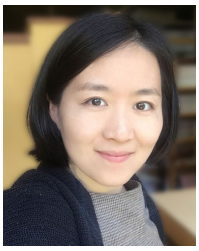

LI WEI (Member, IEEE) received the B.S. degree in electrical engineering and the Ph.D. degree in control theory and control engineering from Tongji University, Shanghai, China, in 2004 and 2010, respectively.

Since 2000, she has been with Tongji University, where she is currently an Associate Professor of electrical engineering with the School of Electronics and Information Engineering. From 2007 to 2008, she was a Visiting Ph.D. Student with the Ecole des Mines de Paris, Sophia Antipolis, France. From 2014 to 2015, she was a Visiting Scientist with RWTH Aachen University, Aachen, Germany. In 2019, she was a Visiting Scientist with Aalborg University, Aalborg, Denmark. Her current research interests include high-power density dc/dc converter for fuel cell vehicle and energy storage application.

Dr. Wei received the Green Talents Award from the German Federal Ministry of Education and Research in 2014.

DIFU ZHAN received the B.S. degree in electrical engineering and automation and the Ph.D. degree in control theory and engineering from Tongji University, in July 2011 and 2016, respectively. After that, he joined Bosch Group as a System Engineer with Bosch (China) Investment Ltd. In 2018, he became a team expert on vehicle power net system development, including high-voltage system engineering for new energy vehicles, redundancy low-voltage power supply system engineering for highly automatic driving vehicles, and onboard electrical energy management. Since 2021, he has been the Director of power electronics with HydraV. His research field during Ph.D. period includes the design and control of high-power dc/dc converters for fuel cell vehicles.

DAN SU received the B.S. and M.S. degrees in electrical engineering from Tongji University, Shanghai, China, in 2005 and 2008, respectively, where he is currently pursuing the Ph.D. degree in power and energy. From 2008 to 2011, he worked as an Electrical Engineer with Murata Power Solution, and developed several standard dc–dc board mounted power supplies in telecom application. Then he worked as a Lead Engineer in GE Power, from 2011 to 2014, and developed standard or customized dc–dc converter for telecom and transportation application. After that, he went to Microchip, in 2015, and worked as a Sr. Application Engineer on digital power supply design and training, with his background and many years' experience in power supply, he help many customers develop their own digital power supply very quickly and successfully. Since 2016, he joined the New Energy and Electrical Apparatus Laboratory, Tongji University, and been responsible for design and manufacture of dc–dc converters used in EV and FCEV. His current research interests include digital control of high-power dc–dc converter in FCEV and energy storage and application of wide band semiconductors.

MINGRUI ZHANG received the B.S., M.S., and Ph.D. degrees in electrical engineering from Tongji University, Shanghai, China, in 1994, 2003, and 2008, respectively. He is currently a Professor with the Department of Electrical Engineering, Tongji University. From 2009 to 2010, he was a Visiting Scholar at Arizona State University, Tucson, AZ, USA, funded by the China Scholarship Council. His current research interests include distributed generation and micro-grids, energy management and optimized operation of electric power systems, and rail transit power systems.